ARTICLE

Structural Investigation of Technetium-Diphosphonate Complex ^{99m}Tc-MDP

Ling Qiu[a*], Jian-guo Lin[a], Xue-hai Ju[b], Xue-dong Gong[b], Shi-neng Luo[a]

a. Key Laboratory of Nuclear Medicine, Ministry of Health, Jiangsu Key Laboratory of Molecular Nuclear Medicine, Jiangsu Institute of Nuclear Medicine, Wuxi 214063, China
b. Institute for Computation in Molecular and Material Science, School of Chemical Engineering, Nanjing University of Science and Technology, Nanjing 210094, China

(Dated: Received on January 11, 2011; Accepted on March 23, 2011)

Density functional theory method has been employed to investigate the structures of the prototypical technetium-labeled diphosphonate complex ^{99m}Tc-MDP, where MDP represents methylenediphosphonic acid. A total of 14 trial structures were generated by allowing for the geometric, conformational, charge, and spin isomerism. Based on the optimized structures and calculated energies at the B3LYP/LANL2DZ level, two stable isomers were determined for the title complex. And they were further studied systematically in comparison with the experimental structure. The basis sets 6-31G*(LANL2DZ for Tc), 6-31G*(cc-pVDZ-pp for Tc), and DGDZVP have also been employed in combination with the B3LYP functional to study the basis set effect on the geometries of isomers. The optimized structures agree well with the available experimental data, and the bond lengths are more sensitive to the basis set than the bond angles. The charge distributions were studied by the Mulliken population analysis and natural bond orbital analysis. The results reflect a significant ligand-to-metal electron donation.

Key words: Radiopharmaceutical, ^{99m}Tc-methylenediphosphonate, Structural prediction, Density functional theory, Basis set effect

I. INTRODUCTION

The technetium-99m-based radiopharmaceuticals have received considerable and increasing attention as diagnostic agents in nuclear medicine due to the favorable nuclear properties (E_γ=142 keV, $t_{1/2}$=6.02 h) and general availability of the radionuclide ^{99m}Tc. They have been used for many years in bone scanning and recently in studying diseases of the heart, brain, kidneys, liver, and other organs as well as tumor tissues [1–4]. Particularly, ^{99m}Tc-labeled diphosphonates, the most widely used radiopharmaceuticals in diagnostic nuclear medicine, provide an effective means of diagnosing primary bone cancer, bone metastases, bone trauma, Paget's disease, *etc* [2–9]. For example, ^{99m}Tc-methylenediphosphonate (^{99m}Tc-MDP, Fig.1) has been reported to be a superior agent for bone imaging [5], which offers significant advantages.

Despite of the importance and widespread clinical use of these agents, almost no definitive information is available to their chemical compositions or structures. Even for the complex ^{99m}Tc-MDP, where MDP is the simplest member of the diphosphonate ligands used in the preparation of ^{99m}Tc bone imaging agents, only one study about its formulation and structure can be found up to date [10]. This is largely because that (i) ^{99m}Tc is available at tracer levels, which does not permit characterization of the complex by routine spectroscopic and analytical methods; (ii) no suitable crystals of these compounds can be obtained for the X-ray structure determination. The lack of fundamental chemical information not only restricts the development of improved ^{99m}Tc-diphosphonates, but also severely hinders the development of analogous diphosphonate formulations containing β-emitting radionuclides such as $^{186/188}$Re, which could be used for the diagnosis and treatment of metastatic bone cancer [2]. Over the past several years, considerable effort has been devoted to understanding the fundamental chemistry of ^{99m}Tc-diphosphonate radiopharmaceuticals [11, 12]. However, these studies do not provide any firm structural data.

As an adjunct to experiment for the design and analysis of novel compounds, molecular modeling has found extensive use in the organic pharmaceuticals and other valuable chemicals [13]. But, it has not yet found wide use in the metal-based diagnostic or therapeutic agents. The challenge arises from well-known difficulties inherent in the transition metal chemistry: large number of electrons and orbitals, relativistic and electron correla-

*Author to whom correspondence should be addressed. E-mail: qiulingwx@gmail.com, Tel.: +86-510-85514482, FAX: +86-510-85513113.

TABLE I Details of molecular mechanics geometry optimization.

Forcefiled	Algorithm	Summation method		Quality		
		Electrostatic	vdW	Energy/(J/mol)	Force/(J/mol)	Displacement/Å
Universal	Smart	Atom based	Atom based	8.36×10^{-2}	4.18	1.0×10^{-5}

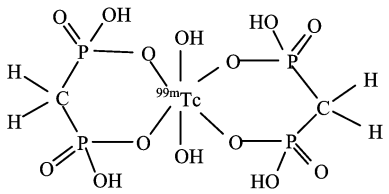

FIG. 1 Schematic illustration of the molecular structure of ^{99m}Tc-MDP.

tion effects, and diverse open-shell species. With tremendous improvement in the computational method and technology, nowadays molecular modeling can be used successfully for the prediction of metal-ligand complex structure, ligand selectivity, coordination number, lipophilicity, and thermodynamic stability. As Jurisson *et al.* stated in the review of coordination compounds in nuclear medicine, "molecular modeling will certainly become an important aspect of the design process" [14].

In this work, molecular modeling was carried out for the structural prediction and understanding the fundamental chemistry of the metal-based diagnostic agent ^{99m}Tc-MDP, which is the prototypical ^{99m}Tc-diphosphonate. Different conformational, geometric, coordination, charge and spin isomers were searched and studied. Two energetically most preferred structures were described and compared with the available experimental data. The effect of basis set was also investigated. These results may be instructive for the design and synthesis of novel ^{99m}Tc-diphosphonate bone imaging agents and other ^{99m}Tc-based radiopharmaceuticals.

II. COMPUTATIONAL METHOD

All the initial models of the complex ^{99m}Tc-MDP were constructed using the 3D build tools as implemented in the Visualizer module of the commercial software materials studio (MS) 3.0.1 [15]. The trial models were optimized by molecular mechanics (MM) method within the Forcite module. Here, it should be introduced that Forcite is a MM module as implemented in MS 3.0.1 for the potential energy calculation and geometry optimization of arbitrary molecular and periodic systems using classical mechanics. It can offer us a wide range of forcefields, such as COMPASS [16], UFF [17], Dreiding [18], and so on. On the other hand, the geometry optimization algorithm offers the steepest descent, conjugate gradient, quasi-Newton, and full Newton-Raphson methods, in addition to the Smart method, which allows very rapid and correct energy minimizations to be performed. In the present work, we carried out the preliminary geometry optimization using the universal forcefield [17], and the details of this process were listed in Table I.

Then, *ab initio* geometry optimizations were carried out on the MM optimized structures of the title complex by using the hybrid density functional theory (DFT) B3LYP (Becke's three parameter nonlocal exchange functional along with the Lee-Yang-Parr correlation functional) [19, 20] method with the program Gaussian 03 [21]. In order to include the technetium-containing model system in the quantum chemical (QM) calculation, the "double-ζ" quality basis set LANL2DZ [22] was chosen here which uses Duning D95V basis set [23] on first row atoms and Los Alamos effective core potential (ECP) plus DZ on Na-Bi [24]. Compared to all-electron basis sets, ECPs account to some extent for relativistic effects, which are believed to become important for the elements from the fourth row of the periodic table. For comparison and investigation of the basis set effect, the basis sets 6-31G*(LANL2DZ for Tc), 6-31G*(cc-pVDZ-pp for Tc), and DGDZVP [25] were also used in combination with the B3LYP functional to study the structures of ^{99m}Tc-MDP. Therein, the standard 6-31G* basis [26] was used for C, H, O, and P atoms, while LanL2DZ and cc-pVDZ-pp [27] were used for Tc respectively in the basis set 6-31G*(LANL2DZ for Tc) and 6-31G*(cc-pVDZ-pp for Tc). Geometries were fully optimized without any symmetry restriction by the Berny method, and the nature of stationary point was verified through the vibrational analysis (no imaginary frequency). The charge distribution of the stable conformations was studied by the Mulliken population analysis (MPA) [28] and natural bond orbital (NBO) analysis [29] as implemented in the Gaussian 03 program package [21].

III. RESULTS AND DISCUSSION

A. Structural prediction

As well known, the first and most important step in any computer-aided design and analysis protocol is to determine reasonable geometries of the target compounds. With respect to the transition metal complex, however, the rational design must also deal with the extra isomeric complexity inherent in the transition metal chemistry. Besides conformational isomers arising from torsion about rotatable bonds, the con-

DOI:10.1088/1674-0068/24/03/295-304

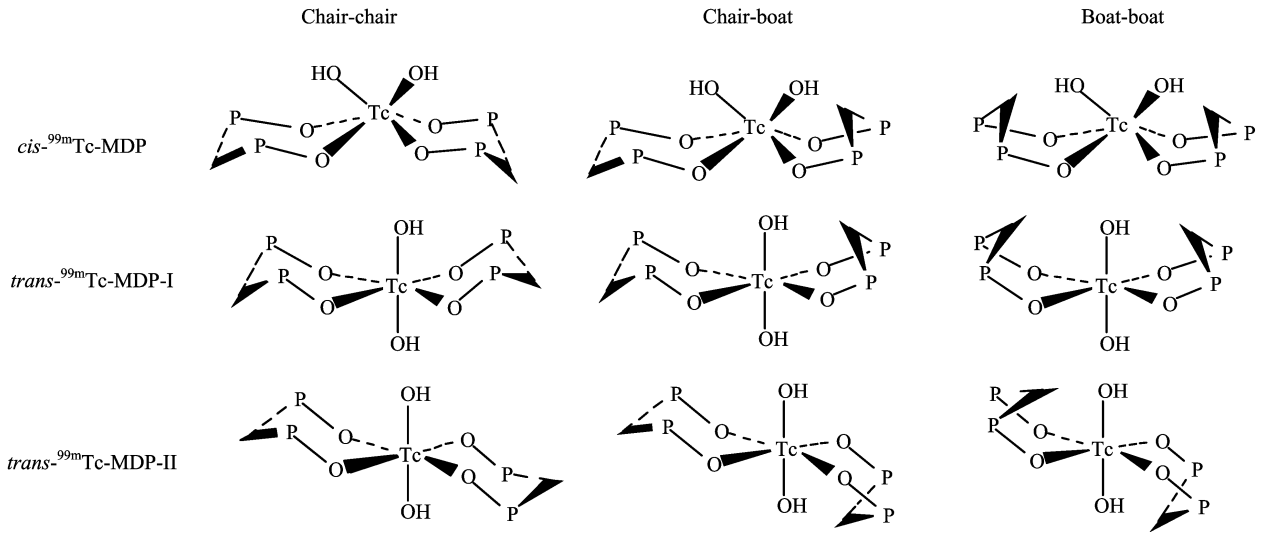

FIG. 2 Schematic illustration of the geometric and conformational isomers predicted for ^{99m}Tc-MDP. Hydrogen and oxygen atoms outside the six-membered ring are omitted for clarity.

formational searching of metal complexes must generate and evaluate (i) geometric isomers (*e.g.*, *cis* versus *trans* octahedral complexes), (ii) structural isomers (*e.g.*, octahedral versus trigonal prismatic for six-coordinate complexes), (iii) coordination isomers (*e.g.*, apical and basal coordination sites for square pyramidal complexes), (iv) spin isomers (typically for open-shell d^2-d^8 electronic configurations). From the computational viewpoint, Tc has a rich "chemical diversity". Inspecting the Cambridge Structural Database (CSD) reveals Tc-complexes in a diverse array of formal oxidation states (-1 to $+7$), coordination numbers (four to eight), ligating atom types (*e.g.*, "soft" phosphorus and sulfur donors, as well as "hard" nitrogen and oxygen donors), and bond types (single to multiple). They also occur in a variety of spin states. Thus, Tc represents a very demanding test of computational methods aimed at effective and efficient structural prediction [30].

At first, extensive search of the lowest-energy structure was conducted for the complex ^{99m}Tc-MDP by considering a number of geometric, structural and coordination isomers. Based on the preliminary MM geometry optimizations performed with the Forcite module, nine unique conformations were obtained as shown in Fig.2. Besides the conformational isomerism arising from those of the ligand MDP (*e.g.*, chair-chair, chair-boat, and boat-boat conformations), these conformations distribute themselves within three classes of geometric isomerism, *i.e.*, *cis*, *trans*-I, and *trans*-II octahedral complexes. Sterically, the *trans* structures are predicted to be lower in the energy than the *cis*, and the *trans*-II are more stable than the *trans*-I.

On the other hand, the oxidation state of Tc is an important parameter during the design of Tc-based pharmaceuticals, which determines the charge and spin state of the corresponding compounds. This may further influence their biological properties significantly. So before *ab initio* QM calculations performed on these structures, charges and spin states of these conformations should be determined. In the case of the six-coordinated ^{99m}Tc-MDP complex, oxidation states +4, +5, +6, and +7 are more possible for the central metal technetium since the oxidation state less than +4 is unstable for Tc [31]. Given an octahedral geometry for Tc(IV) with the electronic configuration [Kr]$4d^3$, duet and quartet spin states are possible. As for Tc(V) with the electronic configuration [Kr]$4d^2$, singlet and triplet spin states are possible, while duet and singlet spin states are possible for [Kr]$4d^1$-Tc(VI) and [Kr]$4d^0$-Tc(VII) respectively. Therefore, total six isomers with different charge and spin can be obtained, *i.e.*, $[^{99m}Tc^{IV}\text{-MDP}]^{2-}$ (S=2), $[^{99m}Tc^{IV}\text{-MDP}]^{2-}$ (S=4), $[^{99m}Tc^{V}\text{-MDP}]^{-}$ (S=1), $[^{99m}Tc^{V}\text{-MDP}]^{-}$ (S=3), $[^{99m}Tc^{VI}\text{-MDP}]$ (S=2), and $[^{99m}Tc^{VII}\text{-MDP}]^{+}$ (S=1). For simplicity of the calculation, the chair-chair conformation of *cis*-^{99m}Tc-MDP was chosen for the QM studies at the B3LYP/LANL2DZ level to evaluate the isomer stability and determine the charge and spin of the title compound. The calculated results were listed in Table II. From Table II, one can see that the total energies E_T of the high spin configurations are smaller than those of low spin configurations, while the dipole moments of the former are larger than those of the latter. For instance, E_T for the quartet spin state of $^{99m}Tc^{IV}$-MDP and triplet spin state of $^{99m}Tc^{V}$-MDP are -1241.6366 and -1241.5518 a.u., respectively; whereas those for the duet spin state of $^{99m}Tc^{IV}$-MDP and singlet spin state of $^{99m}Tc^{V}$-MDP are -1241.6061 and -1241.5429 a.u., respectively. This indicates that the high spin state is more stable than the low spin state for the title compound. It is also noteworthy that E_T increases as the oxidation state of Tc increases from +4 to +7, suggest-

DOI:10.1088/1674-0068/24/03/295-304

TABLE II Total energies (E_T) and dipole moments (μ in Debye) of the various isomers of ^{99m}Tc-MDP calculated at the B3LYP/LANL2DZ level.

Isomer		E_T/a.u.	μ
cis-^{99m}Tc-MDP	$^{-2,2}$Chair-chair[a]	−1241.6061	4.292
	$^{-2,4}$Chair-chair	−1241.6368	4.563
	$^{-1,1}$Chair-chair	−1241.5429	2.560
	$^{-1,3}$Chair-chair	−1241.5518	6.888
	^{0,2}Chair-chair	−1241.3690	5.432
	$^{+1,1}$Chair-chair	−1241.0060	5.005
	$^{-2,4}$Chair-boat	−1241.6324	4.066
	$^{-2,4}$Boat-boat	−1241.6200	2.436
trans-^{99m}Tc-MDP-I	$^{-2,4}$Chair-chair[b]	−1241.6111	5.398
	$^{-2,4}$Chair-boat	−1241.6331	1.509
	$^{-2,4}$Boat-boat	−1241.6194	0.337
trans-^{99m}Tc-MDP-II	$^{-2,4}$Chair-chair	−1241.6385	0.004
	$^{-2,4}$Chair-boat	−1241.6183	3.358
	$^{-2,4}$Boat-boat	−1241.5960	1.863

[a] Isomers with different charge and spin states for the chair-chair conformation of *cis*-^{99m}Tc-MDP, *i.e.*, $[^{99m}Tc^{IV}\text{-MDP}]^{2-}$ (S=2), $[^{99m}Tc^{IV}\text{-MDP}]^{2-}$ (S=4), $[^{99m}Tc^{V}\text{-MDP}]^{-}$ (S=1), $[^{99m}Tc^{V}\text{-MDP}]^{-}$ (S=3), $[^{99m}Tc^{VI}\text{-MDP}]$ (S=2), and $[^{99m}Tc^{VII}\text{-MDP}]^{+}$ (S=1). Superscript at the top left corner denotes the charge and spin state of the complex.

[b] The *trans*-^{99m}Tc-MDP-I chair-chair conformation was destroyed after the geometry optimization, indicating it was not stable.

ing that the conformational stability decreases with the increasing oxidation state of Tc. In addition, inspection of the optimized geometries reveals that the structures with oxidation states Tc(V), Tc(VI), and Tc(VII) change greatly and deviate largely from the expected ideal structures, while those with Tc(IV) state retain the predicted configuration and agree well with the available experimental structure [10]. This further indicates that the former are less stable than the latter. In summary, the most stable conformation of ^{99m}Tc-MDP possesses divalent negative charge (Tc with oxidation state +4) and quartet spin state. This coincides well with the experimental result determined by the potentiometric titration [12].

Therefore, geometry optimizations of other eight conformations shall be performed on the quartet state of $[^{99m}Tc^{IV}\text{-MDP}]^{2-}$ at the B3LYP/LANL2DZ level. Judged from the total electronic energies (Table II), one can see that the conformational stability order is not identical within each class of geometric isomers. As for the *cis*- and *trans*-II-classes, the stability both decreases in the order of chair-chair>chair-boat>boat-boat, while that of the *trans*-I class decreases in the order of chair-boat>boat-boat>chair-chair. Here, it should be pointed out that during the geometry optimization process, any attempt to model the chair-chair form of *trans*-^{99m}Tc-MDP-I led to an irrational collapsed structure. This implies that this form is untenable from the electronic point of view although it is sterically reasonable. Moreover, the stability also changes in a different sequence within three classes of conformational isomers relative to the ligand MDP. For example, as for the chair-chair conformation, the stability decreases in the order of *trans*-II>*cis*>*trans*-I, as for the chair-boat conformation, that decreases in the order of *trans*-I>*cis*>*trans*-II, and as for the boat-boat conformation, that decreases in the order of *cis*>*trans*-I>*trans*-II.

Based on an overall consideration of various factors, *cis*-chair-chair and *trans*-II-chair-chair conformations were thought to be the preferred stable isomers of ^{99m}Tc-MDP. However, the energy difference between these two conformations was very small (ΔE=4.48 kJ/mol), so we formulated the hypothesis that ^{99m}Tc-MDP may exist as a complicated mixture of *cis*- and *trans*-chair-chair conformers. Hence, the *cis* and *trans* isomers with the lowest energy were selected for the subsequent studies.

B. Comparison between experimental and theoretical geometries

Besides the B3LYP/LANL2DZ spin-unrestricted geometry optimization, the B3LYP in combination with three other basis sets, 6-31G*(LANL2DZ for Tc), 6-31G*(cc-pVDZ-pp for Tc), and DGDZVP, was also used to optimize the *cis* and *trans* isomers of ^{99m}Tc-MDP. For clarity, only the structures optimized at the B3LYP/LANL2DZ level were shown in Fig.3. Selected geometric parameters calculated at different levels were presented in Tables III and IV as well as the available experimental data reported for the complex $[Li(H_2O)_3][^{99m}Tc^{IV}(OH)(MDP)]\cdot 1/3H_2O$ [10].

As depicted in Fig.3, the framework exhibits an octahedral coordination sphere about Tc although no crystallographic symmetry is imposed, and two bridging oxygen atoms from the hydroxyl occupy the *cis*- and *trans*-coordination sites respectively in the *cis* and *trans* isomers. As for the *cis* isomer, the basal plane is defined by four oxygen atoms (O2, O6, O11, and O21) of the MDP and hydroxy ligands, and the apical positions are occupied by another two oxygen atoms (O7 and O20) of the MDP and hydroxy ligands. As for the *trans* isomer, the basal plane is defined by four oxygen atoms from the MDP ligands (O2, O6, O7, and O11), while the apical positions are occupied by two oxygen atoms from the hydroxy ligands (O20 and O21).

From Tables III and IV, several features can be observed. First, the calculated Tc−O bond lengths in the *cis* isomer range from 1.999 Å to 2.104 Å and those in the *trans* isomer range from 2.020 Å to 2.066 Å, which are generally in line with the observed Tc−O single bond lengths (2.00−2.03 Å) [32] since Tc=O double

DOI:10.1088/1674-0068/24/03/295-304

TABLE III Selected bond lengths (Å) calculated for ^{99m}Tc-MDP at different levels in comparison with experimental data. A, B, C, and D denote the calculations at the B3LYP/LANL2DZ, B3LYP/6-31G*(LANL2DZ for Tc), B3LYP/6-31G*(cc-pVDZ-pp for Tc), and B3LYP/DGDZVP levels, respectively.

Bond	Ref.[10]	*cis*-^{99m}Tc-MDP				*trans*-^{99m}Tc-MDP			
		A	B	C	D	A	B	C	D
Tc1−O2	2.000(14)	2.007	2.023	2.020	2.076	2.020	2.029	2.024	2.047
Tc1−O6	2.036(16)	2.019	2.042	2.035	2.086	2.020	2.029	2.024	2.047
Tc1−O7	1.983(14)	2.007	2.043	2.036	2.039	2.020	2.029	2.024	2.047
Tc1−O11	2.029(12)	2.019	2.061	2.051	2.104	2.020	2.029	2.024	2.047
Tc1−O20	1.968(15)	2.088	2.035	2.027	2.022	2.066	2.049	2.038	2.058
Tc1−O21	1.917(12)	2.088	2.019	2.011	1.999	2.066	2.049	2.038	2.058
P3−O2	1.552(14)	1.677	1.578	1.578	1.569	1.677	1.584	1.583	1.580
P3−O12	1.502(18)	1.589	1.493	1.493	1.495	1.590	1.492	1.492	1.493
P3−O13	1.552(15)	1.710	1.627	1.628	1.622	1.707	1.623	1.623	1.626
P5−O6	1.534(15)	1.677	1.582	1.581	1.552	1.677	1.584	1.583	1.580
P5−O14	1.460(16)	1.589	1.493	1.493	1.502	1.590	1.492	1.492	1.493
P5−O15	1.551(14)	1.710	1.627	1.627	1.673	1.707	1.623	1.623	1.626
P8−O7		1.677	1.558	1.557	1.548	1.677	1.584	1.583	1.580
P8−O16		1.589	1.498	1.498	1.501	1.590	1.492	1.492	1.493
P8−O17		1.710	1.673	1.672	1.676	1.707	1.623	1.623	1.626
P10−O11		1.677	1.580	1.579	1.576	1.677	1.584	1.583	1.580
P10−O18		1.589	1.493	1.493	1.494	1.590	1.492	1.492	1.493
P10−O19		1.710	1.614	1.616	1.618	1.707	1.623	1.623	1.626
C4−P3	1.83(2)	1.886	1.846	1.846	1.854	1.885	1.844	1.844	1.843
C4−P5	1.78(2)	1.882	1.840	1.841	1.827	1.885	1.844	1.844	1.843
C9−P8		1.886	1.828	1.828	1.830	1.885	1.844	1.844	1.843
C9−P10		1.882	1.850	1.851	1.850	1.885	1.844	1.844	1.843

bond lengths are considerably shorter (1.65−1.70 Å) [32]. Compared with the experimental values ranging from 1.917 Å to 2.036 Å, the optimized Tc−O bond distances are slightly longer and the *cis* structure shows better agreement with the X-ray results [10]. This is not surprising given that crystal packing and hydrogen bonds can induce conformational features that are not present in the theoretical calculation of the isolated molecule in the gas phase at 0 K, and the X-ray diffraction data is only directed to the *cis* isomer instead of the *trans* isomer that has not been reported yet. Additionally, there are inherent errors in the DFT calculations. The best calculated results for the Tc−O bond were obtained using the basis set 6-31G*(cc-pVDZ-pp for Tc) with the largest deviation of 0.094 and 0.121 Å for the *cis* and *trans* isomers respectively. All the other methods overestimate these bond lengths more. This indicates that the gaseous and solid structure represents a good approximation at the B3LYP/6-31G*(cc-pVDZ-pp for Tc) level, namely, this method is more suitable for studying the title complex. Moreover, there are 15 bond angles about Tc in the title complex with the coordination mode MA_4B_2. Three of them have equilibrium values of 180°, and the rest have equilibrium values of 90°. The B−M−B bond angle, *i.e.*, O20−Tc1−O21, has the equilibrium value of 90° in the *cis* form and 180° in the *trans*, see Table IV. As the basis set changing from LANL2DZ to DGDZVP, the optimized bond angles about Tc change slightly. That is, the basis set has little effect on these bond angles.

On the other hand, bond lengths and bond angles within the MDP ligand are generally as expected from structural studies on the free acid H_4MDP [33] and related diphosphonate salts [37–39]. The P−O bond lengths fall into two distinct classes. The longer ones *i.e.*, P3−O2, P3−O13, P5−O6, P5−O15, P8−O7, P8–O17, P10–O11, and P10–O19 ranging from 1.548 Å to 1.71 Å represent P−O single bonds 1.545−1.548 Å [36] while the remaining ones (3−O12, P5−O14, P8−O16, and P10−O18) ranging from 1.492 Å to 1.502 Å shows considerable double bond character (1.494–1.5 Å) [33]. It is noteworthy that the P−O and P=O bond lengths are both sensitive to the basis set. In comparison with the calculated results of the LANL2DZ basis set, the use of 6-31G*(LANL2DZ for Tc, cc-pVDZ-pp for Tc) and DGDZVP basis sets leads to a remarkable decrease of the P−O and P=O lengths, which are more consistent with the experimental data [10]. Especially as the basis set 6-31G*(LANL2DZ for Tc or cc-pVDZ-pp for Tc) was used, the values are closer to the experimen-

DOI:10.1088/1674-0068/24/03/295-304

TABLE IV Selected bond angles (°) of ^{99m}Tc-MDP calculated at different levels in comparison with experimental data. A, B, C, and D denote the calculations at the B3LYP/LANL2DZ, B3LYP/6-31G*(LANL2DZ for Tc), B3LYP/6-31G*(cc-pVDZ-pp for Tc), and B3LYP/DGDZVP levels, respectively.

Angle	Ref.[10]	*cis*-^{99m}Tc-MDP				*trans*-^{99m}Tc-MDP			
		A	B	C	D	A	B	C	D
O2−Tc1−O6		90.33	89.29	89.11	88.56	86.16	87.59	87.35	86.70
O2−Tc1−O7		92.75	91.55	91.71	91.94	180.00	180.00	180.00	180.00
O2−Tc1−O11		96.76	92.06	92.09	92.44	93.84	92.41	92.65	93.30
O2−Tc1−O20		88.29	89.00	88.87	88.98	89.86	90.00	90.20	89.47
O2−Tc1−O21		176.23	178.90	177.90	177.30	90.13	90.00	89.79	90.52
O6−Tc1−O7		96.78	91.50	90.67	89.53	93.83	92.41	92.64	93.30
O6−Tc1−O11		169.73	177.40	178.60	177.50	180.00	180.00	180.00	180.00
O6−Tc1−O20		86.84	89.72	89.92	89.66	89.85	89.99	90.20	89.47
O6−Tc1−O21		85.94	90.74	90.87	88.93	90.17	90.02	89.81	90.53
O7−Tc1−O11		90.31	90.70	90.11	88.16	86.17	87.59	87.35	86.70
O7−Tc1−O20		176.23	178.70	179.20	178.80	90.15	90.02	89.81	90.53
O7−Tc1−O21		88.29	89.54	90.36	88.92	89.86	89.99	90.20	89.47
O11−Tc1−O20		85.95	88.07	89.29	92.63	90.13	90.00	89.79	90.52
O11−Tc1−O21		86.85	87.87	87.90	90.11	89.85	90.00	90.20	89.47
O20−Tc1−O21		90.90	89.90	89.06	90.13	180.00	180.00	180.00	180.00
O2−P3−O12	109.9(9)	117.83	117.15	117.19	117.84	117.58	116.36	116.45	116.57
O2−P3−O13	111.1(8)	103.93	105.70	105.79	106.95	104.20	105.98	106.03	106.19
O12−P3−O13	108.9(9)	112.77	111.72	111.53	111.57	113.12	112.10	112.00	111.55
O6−P5−O14	114.4(9)	117.45	116.39	116.45	117.64	117.58	116.36	116.45	116.57
O6−P5−O15	110.1(8)	103.13	105.74	105.81	105.73	104.20	105.98	106.04	106.19
O14−P5−O15	111.1(9)	112.26	111.46	111.49	107.46	113.12	112.10	112.00	111.55
O7−P8−O16		117.84	117.30	117.26	118.28	117.58	116.36	116.45	116.57
O7−P8−O17		103.94	106.02	106.03	105.84	104.20	105.98	106.04	106.19
O16−P8−O17		112.76	108.03	108.15	107.51	113.12	112.10	112.00	111.55
O11−P10−O18		117.44	116.71	116.88	116.94	117.59	116.36	116.45	116.57
O11−P10−O19		103.15	106.40	106.41	106.96	104.20	105.98	106.03	106.19
O18−P10−O19		112.26	112.49	112.36	111.82	113.11	112.10	112.00	111.55
C4−P3−O2	108.4(10)	105.35	105.63	105.69	105.53	104.81	105.25	105.25	105.72
C4−P3−O12	111.9(10)	111.20	110.54	110.54	108.97	111.05	110.72	110.79	110.53
C4−P3−O13	106.6(10)	104.62	105.26	105.27	105.09	104.97	105.67	105.52	105.55
C4−P5−O6	106.7(9)	105.16	105.33	105.30	108.01	104.81	105.25	105.25	105.72
C4−P5−O14	110.4(10)	111.74	111.18	111.25	113.01	111.05	110.72	110.79	110.53
C4−P5−O15	103.4(9)	106.11	106.02	105.78	103.86	104.97	105.67	105.53	105.55
C9−P8−O7		105.34	107.98	107.85	108.05	104.82	105.25	105.25	105.72
C9−P8−O16		111.21	113.25	113.39	112.74	111.04	110.72	110.79	110.53
C9−P8−O17		104.61	103.09	102.96	103.12	104.97	105.67	105.53	105.55
C9−P10−O11		105.17	104.84	105.01	105.12	104.81	105.25	105.25	105.72
C9−P10−O18		111.74	109.86	109.89	109.52	111.05	110.72	110.79	110.53
C9−P10−O19		106.10	105.74	105.45	105.72	104.97	105.67	105.52	105.55
P3−C4−P5	110.7(12)	119.72	120.16	120.30	120.79	119.19	120.13	120.19	120.76
P8−C9−P10		119.72	120.59	120.52	120.79	119.20	120.13	120.19	120.76

tal data. A similar phenomenon was observed for the C−P bond, which was also sensitive to the basis set, and those obtained from 6-31G*(LANL2DZ for Tc or cc-pVDZ-pp for Tc) basis set agreed more with the experimental value.

The coordination around the P atom is approximately tetrahedral with small deviations induced by the different environment of the oxygen atom. This can

DOI:10.1088/1674-0068/24/03/295-304

TABLE V Energies and dipole moments of the stable *cis*- and *trans*-^{99m}Tc-MDP conformations calculated at different levels of DFT theory. E_T, E_H, E_L, and ΔE_g denote the total electronic energy, energy of the highest occupied molecular orbital (HOMO), energy of the lowest unoccupied molecular orbital (LUMO), and the energy gap between HOMO and LUMO, respectively, with the units in a.u. μ is in Debye.

Methods	Conformation	E_T	E_H	E_L	ΔE_g	μ
B3LYP/LANL2DZ	*cis*-^{99m}Tc-MDP	−1241.6368	−0.043	0.085	0.127	4.564
	trans-^{99m}Tc-MDP	−1241.6385	−0.042	0.078	0.119	0.004
B3LYP/6-31G*	*cis*-^{99m}Tc-MDP	−2581.3577	−0.016	0.114	0.130	5.149
(LANL2DZ for Tc)	*trans*-^{99m}Tc-MDP	−2581.3709	−0.026	0.101	0.126	0.002
B3LYP/6-31G*	*cis*-^{99m}Tc-MDP	−2581.9049	−0.009	0.127	0.137	5.284
(cc-pVDZ-pp for Tc)	*trans*-^{99m}Tc-MDP	−2581.9179	−0.019	0.114	0.133	0.001
B3LYP/DGDZVP	*cis*-^{99m}Tc-MDP	−6707.9711	−0.036	0.095	0.131	7.274
	trans-^{99m}Tc-MDP	−6707.9964	−0.051	0.071	0.122	0.002

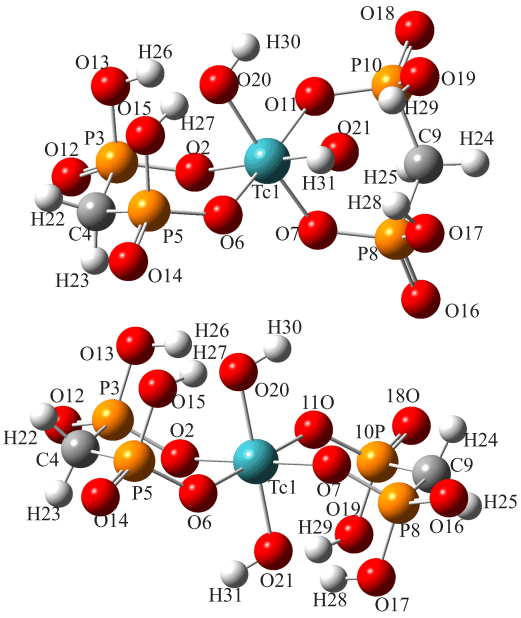

FIG. 3 Optimized structures of the stable *cis*- (up) and *trans*-^{99m}Tc-MDP (down) at the B3LYP/LANL2DZ level, showing one Tc center bridging two MDP ligands.

be indicated by the bond angles O−P−O and C−P−O given in Table IV. However, It is noteworthy that the O−P−O and C−P−O bond angles involving O12, O14, O16, and O18 with the average values of 117.18° and 111.16° are obviously larger than others with the average values of 108.56° and 105.39° respectively. The basis set has little effect on these bond angles.

In addition, one of the most important structural features of the diphosphonate ligands is the orientation of the $-PO_3$ groups with respect to the P−C−P plane. The atoms O12−P3−C4−P5−O14 (O16−P8−C9−P10−O18) form a planar "W" configuration (see Fig.3), which accord well with the previously experimental and theoretical studies [10, 34–38]. This configuration allows the ligand to be doubly bidentate with O2 and O6 on one side of the "W" coordinating to one metal center and O13 and O15 on the other side of the "W" coordinating to another metal center.

On the whole, the theoretically calculated bond lengths and bond angles of ^{99m}Tc-MDP are in reasonable agreement with the crystallographic data. In other words, the structural information observed in the X-ray diffraction study can be well reproduced by the present DFT calculations especially at the B3LYP/6-31G*(cc-pVDZ-pp for Tc) level.

C. Electronic structure

The DFT calculations were further carried out at four different levels to study the electronic structure of the stable *cis* and *trans* isomers. Table V lists the energies of total electron and frontier molecular orbitals (FMOs) (HOMO, highest occupied molecular orbital, LUMO, lowest unoccupied molecular orbital), energy gap between FMOs (ΔE_g=E_L−E_H) and dipole moment (μ). The charge distribution and spin density obtained from the MPA and NBO analyses are given in Table VI.

As can be seen from Table V, at four computational levels the total energy and dipole moment of the *cis* isomer are all larger than those of the *trans*. Hence it follows that the *cis* form is less stable than the t*rans* one and the molecular polarity of the former is larger than the latter. This is in line with the molecular symmetry of the optimized structure (the *trans* isomer with C_{2h} symmetry while the *cis* with C_1 symmetry). However, the FMO energies and energy gaps ΔE_g of the *cis* isomer are larger than those of the *trans* on the whole, indicating that the former has higher stability than the latter. Here the stability refers to the chemical or photochemical processes with electron transfer or leap. As the basis set varying from LANL2DZ to DGDZVP, the total energies of *cis* and *trans* isomers both decrease, while the dipole moment of the *cis* increases from 4.564 Debye to 7.274 Debye and the *trans* almost possesses no dipole moment due to the C_{2h} symmetry. The whole FMO energies and energy gaps are shifted to higher values in the mass.

DOI:10.1088/1674-0068/24/03/295-304

TABLE VI Atomic charge and spin density from NPA and MPA analyses for the stable cis- and trans-^{99m}Tc-MDP at different DFT levels. A, B, C, and D denote the calculations at the B3LYP/LANL2DZ, B3LYP/6-31G*(LANL2DZ for Tc), B3LYP/6-31G*(cc-pVDZ-pp for Tc), and B3LYP/DGDZVP levels, respectively.

NPA	*cis*-^{99m}Tc-MDP				*trans*-^{99m}Tc-MDP			
	A	B	C	D	A	B	C	D
Q_{Tc1}	1.624	1.608	1.760	1.973	1.635	1.589	1.743	1.943
Q_{O2}	−0.996	−1.031	−1.059	−1.104	−1.028	−1.033	−1.059	−1.095
Q_{O6}	−1.037	−1.027	−1.055	−1.109	−1.028	−1.033	−1.059	−1.095
Q_{O7}	−0.996	−1.036	−1.059	−1.113	−1.028	−1.033	−1.059	−1.095
Q_{O11}	−1.037	−1.048	−1.065	−1.081	−1.028	−1.033	−1.059	−1.095
Q_{O20}	−1.046	−0.984	−1.002	−1.002	−1.026	−0.991	−1.013	−1.080
Q_{O21}	−1.046	−0.961	−0.988	−1.029	−1.026	−0.991	−1.013	−1.080
Q_{P3}	2.290	2.420	2.427	2.428	2.292	2.425	2.426	2.426
Q_{O12}	−1.065	−1.112	−1.121	−1.158	−1.071	−1.112	−1.115	−1.145
Q_{O13}	−1.058	−1.064	−1.065	−1.072	−1.061	−1.064	−1.064	−1.065
Q_{C4}	−1.176	−1.300	−1.298	−1.167	−1.177	−1.300	−1.299	−1.164
MPA	*cis*-^{99m}Tc-MDP				*trans*-^{99m}Tc-MDP			
	A	B	C	D	A	B	C	D
Q_{Tc1}	1.292	1.222	0.758	1.262	1.278	1.196	0.739	1.257
Q_{O2}	−0.746	−0.699	−0.647	−0.711	−0.751	−0.704	−0.653	−0.715
Q_{O6}	−0.758	−0.704	−0.651	−0.694	−0.751	−0.704	−0.653	−0.715
Q_{O7}	−0.746	−0.668	−0.622	−0.694	−0.751	−0.704	−0.653	−0.715
Q_{O11}	−0.758	−0.702	−0.655	−0.698	−0.751	−0.704	−0.653	−0.715
Q_{O20}	−0.817	−0.842	−0.814	−0.842	−0.821	−0.846	−0.823	−0.948
Q_{O21}	−0.817	−0.827	−0.776	−0.867	−0.821	−0.846	−0.823	−0.948
Q_{P3}	1.348	1.184	1.199	1.263	1.348	1.183	1.209	1.262
Q_{O12}	−0.725	−0.609	−0.602	−0.677	−0.730	−0.605	−0.599	−0.670
Q_{O13}	−0.744	−0.756	−0.764	−0.777	−0.749	−0.752	−0.762	−0.775
Q_{C4}	−0.890	−0.704	−0.709	−0.918	−0.895	−0.704	−0.710	−0.923
ρ_{Tc1}	2.527	2.600	2.671	2.671	2.572	2.613	2.682	2.682
ρ_{O2}	0.106	0.076	0.061	0.054	0.073	0.064	0.049	0.049
ρ_{O6}	0.074	0.068	0.049	0.017	0.073	0.064	0.049	0.049
ρ_{O7}	0.106	0.053	0.041	0.030	0.073	0.064	0.049	0.049
ρ_{O11}	0.074	0.052	0.042	0.051	0.073	0.064	0.049	0.049
ρ_{O20}	0.017	0.033	0.025	0.067	0.023	0.033	0.026	0.028
ρ_{O21}	0.017	0.054	0.040	0.052	0.023	0.033	0.026	0.028
ρ_{P3}	0.004	0.003	0.005	0.004	0.006	0.004	0.006	0.005
ρ_{O12}	-0.002	0.000	0.000	0.000	−0.001	−0.001	−0.001	−0.002
ρ_{O13}	0.007	0.005	0.004	0.007	0.006	0.004	0.003	0.005
ρ_{C4}	0.007	0.004	0.004	0.004	0.008	0.005	0.004	0.006

By focusing on the atomic charges of the stable *cis* and *trans* isomers, we first consider the NPA (natural population analysis) [39] charge distributions (Table VI). For both isomers, non-negligible negative charges (ca. −1.0) are found on the oxygen atoms which are coordinated to the technetium (*i.e.*, O2, O6, O7, O11, O20, and O21), and the metal atom technetium carries a relatively large positive charge (from 1.589 to 1.973) which is considerable lower than the formal charge of +4. This is the product of a significant electron donation from the MDP and hydroxyl ligands. The atoms bonded to the phosphorus (*i.e.*, O12, O13, and C4) also carry relatively large negative charges (ca. −1.1 and ca. −1.2−−1.3) and the phosphorus possesses a large positive charge (ca. 2.3–2.4), which is also considerable smaller than the formal charge of +5. This also reflects a significant oxygen-to-phosphorus electron donation.

With the basis set changing from LANL2DZ to DGDZVP, the charge on Tc of the *cis* isomer initially decreases from 1.624 at LANL2DZ to 1.608 at 6-31G*(LANL2DZ for Tc) and then increases to 1.760

DOI:10.1088/1674-0068/24/03/295-304

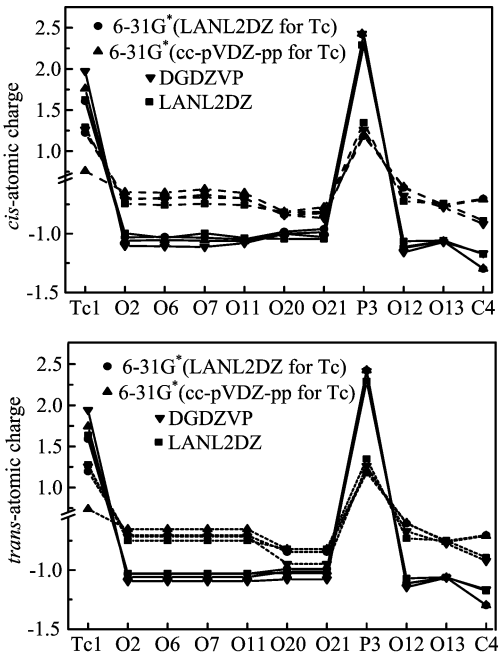

FIG. 4 Atomic charges of the *cis*- and *trans*-^{99m}Tc-MDP calculated at different levels of DFT theory. Solid lines and dashed lines represent the NBO and MPA results, respectively.

at 6-31G*(cc-pVDZ-pp for Tc) to 1.973 at DGDZVP. On the contrary, those on the O atoms of the hydroxy ligands increase initially and then decrease at the corresponding calculation level. And those on the O atoms of the MDP ligand (O2, O6, O7, O11) and those bonding with the phosphorus (O12, O13) all decrease on the whole with the changing basis set. The atomic charge of P monotonically increases from 2.29 at LANL2DZ to 2.43 at DGDZVP. Similar features were also observed for the *trans* isomer. The atomic charge of Tc initially decreases from 1.635 at LANL2DZ to 1.589 at 6-31G*(LANL2DZ for Tc) and then increases to 1.743 at 6-31G*(cc-pVDZ-pp for Tc) to 1.943 at DGDZVP. Those on the O atoms of the hydroxy ligands increase from LANL2DZ to 6-31G*(LANL2DZ for Tc) and then decrease to 6-31G*(cc-pVDZ-pp for Tc) to DGDZVP, and those on the O atoms of the MDP ligand and those bonding with the phosphorus all decrease monotonically with the basis set changing. The atomic charge of P also increases from 2.29 at LANL2DZ to 2.43 at DGDZVP.

Also it is noteworthy that the charge distribution on the *trans* isomer is completely symmetrical at four calculation levels while that on the *cis* isomer is not symmetrical, which accord well with the symmetry analysis of the optimized geometries.

As given by MPA, the atomic net charges of both isomers are all smaller than those of NPA and the metallic net charges are also much smaller than its formal +4 oxidation state, reflecting a significant ligand-to-metal electron donation. It follows that the concept of formal charges should not be taken as measure for the actual partial charge of the metal atom. With the basis set changing, the nonmonotonic variations of the MPA charges are not consistent with those of the NPA ones, but they are consistent with each other for the *cis* and *trans* isomers on the whole. The atomic charges of Tc initially decrease from LANL2DZ to 6-31G*(LANL2DZ for Tc) to 6-31G*(cc-pVDZ-pp for Tc) and then increase to DGDZVP, while those of the O atoms of the MDP ligand increase initially from LANL2DZ to 6-31G*(cc-pVDZ-pp for Tc) and then decrease to DGDZVP. The partial charges of other atoms fluctuate irregularly with the basis set changing. This may be attributed to the MPA intrinsic shortcomings such as the basis set dependence [28]. On the whole, the absolute values of MPA charges obtained by B3LYP/6-31G*(cc-pVDZ-pp for Tc) are particularly lower than other methods. These electronic features can also be observed intuitively from Fig.4.

In addition, MPA spin-unrestricted analysis also provides the atomic spin density ρ, which is the difference between the total α and β electronic populations of the atom. It can be found that the spin densities in *cis* and *trans* isomers are both mainly localized on the center metal Tc (ca. 2.6) and some spin densities are located on the six coordinated oxygen atoms (Table VI). On the other atoms those are not directly coordinated to the metal Tc, there is little spin density. This shows that the spin density is borne by the technetium atom and corresponds to the quartet d^3 state of the technetium atom in the title complex, implying that no metal-ligand back-donation exists at this level. As the basis set increasing, the spin densities on Tc increase slightly while those on the O atoms of the MDP ligand decrease on the whole.

IV. CONCLUSION

In this work, a detailed density functional theory study has been performed to predict and investigate the structures of the clinically widely-used bone imaging agent ^{99m}Tc-MDP. The major findings can be summarized as follows:

Although a total of 14 isomers can be generated allowing for the geometric, conformational, charge and spin isomerism, two most energetically preferred structures are determined for the title complex by the DFT-B3LYP/LANL2DZ calculation: *cis*-chair-chair and *trans*-II-chair-chair conformations with divalent negative charge [Tc^{4+}] and quartet spin state. ^{99m}Tc-MDP may exist as a complicated mixture of *cis* and *trans* isomers since their energy difference is very small (ΔE=4.48 kJ/mol).

The B3LYP functional in conjunction with the basis set LANL2DZ, 6-31G*(LANL2DZ for Tc, cc-pVDZ-pp for Tc), and DGDZVP can generate reliable geometries of the title complex. The bond lengths are more sensitive to the basis set than the bond angles, and

DOI:10.1088/1674-0068/24/03/295-304

most bond lengths are generally more overestimated by B3LYP/LANL2DZ than other methods. B3LYP/6-31G*(cc-pVDZ-pp for Tc) optimized geometries agree better with the available experimental data on the whole.

The MPA and NPA charge distributions are both in line with the molecular symmetries C_1 and C_{2h} of the optimized *cis* and *trans* isomer structures, and they both reflect a significant ligand-to-metal electron donation. With the basis set changing, the nonmonotonic variations of MPA charges are not consistent with those of NPA, but they are consistent with each other for the *cis* and *trans* isomers in general.

V. ACKNOWLEDGMENTS

This work was supported by the National Natural Science Foundation of China (No.20801024 and No.21001055), the Natural Science Foundation of Jiangsu Province (No.BK2009077), and the Science Foundation of Health Department of Jiangsu Province (No.H200963).

[1] P. Valk, J. McRae, A. J. Bearden, and P. Hambright, J. Chem. Educ. **53**, 542 (1976).
[2] E. K. Pauwels and M. P. Stokkel, Q. J. Nucl. Med. **45**, 18 (2001).
[3] C. Love, A. S. Din, M. B. Tomas, T. P. Kalapparambath, and C. J. Palestro, Radiographics. **23**, 341 (2003).
[4] M. D. Bartholom, A. S. Louie, J. F. Valliant, and J. Zubieta, Chem. Rev. **110**, 2903 (2010).
[5] G Subramanian, J. G. McAfee, R. J. Blair, F. A. Kallfelz, and F. D. Thomas, J. Nucl. Med. **16**, 744 (1975).
[6] J. A. Bevan, A. J. Tofe, J. J. Benedict, M. D. Francis, and B. L. Barnett, J. Nucl. Med. **21**, 961 (1980).
[7] B. J. Fueger, M. Mitterhauser, W. Wadsak, S. Ofluoglu, T. Traub, G. Karanikas, R. Dudczak, and C. Pirich, Nucl. Med. Commun. **25**, 361 (2004).
[8] E. Palma, B. L. Oliveira, J. D. Correia, L. Gano, L. Maria, I. C. Santos, and I. J. Santos, Biol. Inorg. Chem. **12**, 667 (2007).
[9] J. G. Lin, S. N. Luo, C. Q. Chen, L. Qiu, Y. Wang, W. Cheng, W. Z. Ye, and Y. M. Xia, Appl. Radiat. Isotopes. **68**, 1616 (2010).
[10] K. Libson, E. Deutsch, and B. L. Barnett, J. Am. Chem. Soc. **102**, 2476 (1980).
[11] J. L. Martin Jr., J. Yuan, C. E. Lunte, R. C. Elder, W. R. Heineman, and E. Deutsch, Inorg. Chem. **28**, 2899 (1989).
[12] T. G. Tji, H. A. Vink, W. J. Gelsema, and C. L. De Ligny, Appl. Radiat. Isotopes. **41**, 17 (1990).
[13] K. X. Chen, H. L. Jiang, and R. Y. Ji, *Computer Aided Drug Design, 1st Edn.*, Shanghai: Shanghai Scientific and Technology Press, (2000).
[14] S. Jurisson, D. Berning, W. Jia, and D. S. Ma, Chem. Rev. **93**, 1137 (1993).
[15] Materials Studio 3.0.1, San Diego, CA: Accelrys Inc., (2004).
[16] H. Sun, J. Phys. Chem. B **102**, 7338 (1998).
[17] A. K. Rapp, C. J. Casewit, K. S. Colwell, W. A. Goddard, and W. M. Skiff, J. Am. Chem. Soc. **114**, 10024 (1992).
[18] S. L. Mayo, B. D. Olafson, and W. A. Goddard, J. Phys. Chem. **94**, 8897 (1990).
[19] A. D. Becke, J. Chem. Phys. **98**, 5648 (1993).
[20] C. Lee, W. Yang, and R. G. Parr, Phys. Rev. B **37**, 785 (1988).
[21] M. J. Frisch, G. W. Trucks, H. B. Schlegel, G. E. Scuseria, M. A. Robb, J. R. Cheeseman, J. A. Montgomery, Jr., T. Vreven, K. N. Kudin, J. C. Burant, J. M. Millam, S. S. Iyengar, J. Tomasi, V. Barone, B. Mennucci, M. Cossi, G. Scalmani, N. Rega, G. A. Petersson, H. Nakatsuji, M. Hada, M. Ehara, K. Toyota, R. Fukuda, J. Hasegawa, M. Ishida, T. Nakajima, Y. Honda, O. Kitao, H. Nakai, M. Klene, X. Li, J. E. Knox, H. P. Hratchian, J. B. Cross, C. Adamo, J. Jaramillo, R. Gomperts, R. E. Stratmann, O. Yazyev, A. J. Austin, R. Cammi, C. Pomelli, J. W. Ochterski, P. Y. Ayala, K. Morokuma, G. A. Voth, P. Salvador, J. J. Dannenberg, V. G. Zakrzewski, S. Dapprich, A. D. Daniels, M. C. Strain, O. Farkas, D. K. Malick, A. D. Rabuck, K. Raghavachari, J. B. Foresman, J. V. Ortiz, Q. Cui, A. G. Baboul, S. Clifford, J. Cioslowski, B. B. Stefanov, G. Liu, A. Liashenko, P. Piskorz, I. Komaromi, R. L. Martin, D. J. Fox, T. Keith, M. A. Al-Laham, C. Y. Peng, A. Nanayakkara, M. Challacombe, P. M. W. Gill, B. Johnson, W. Chen, M. W. Wong, C. Gonzalez, and J. A. Pople, *Gaussian 03* (Revision C.02), Wallingford CT: Gaussian, Inc., (2004).
[22] P. J. Hay and W. R. Wadt, J. Chem. Phys. **82**, 299 (1985).
[23] T. H. Dunning Jr. and P. J. Hay, *Modern Theoretical Chemistry*, New York: Plenum, 3, 1 (1976).
[24] P. J. Hay and W. R. Wadt, J. Chem. Phys. **82**, 270 (1985).
[25] N. Godbout, D. R. Salahub, J. Andzelm, and E. Wimmer, Can. J. Chem. **70**, 560 (1992).
[26] P. C. Hariharan and J. A. Pople, Theor. Chim. Acta **28**, 213 (1973).
[27] K. A. Peterson, D. Figgen, M. Dolg, and H. Stoll, J. Chem. Phys. **126**, 124101 (2007).
[28] R. S. Mulliken, J. Chem. Phys. **23**, 1833 (1955).
[29] J. P. Foster and F. Weinhold, J. Am. Chem. Soc. **102**, 7211 (1980).
[30] C. Buda, S. K. Burt, T. R. Cundari, and P. S. Shenkin, Inorg. Chem. **41**, 2060 (2002).
[31] X. B. Wang and J. F. Chu, J. Isotopes. **16**, 35 (2003).
[32] R. W. Thomas, G. W. Estes, R. C. Elder, and E. Deutsch, J. Am. Chem. Soc. **101**, 4581 (1979).
[33] D. DeLaMatter, J. J. McCullough, and C. Calvo, J. Phys. Chem. **77**, 1146 (1973).
[34] V. A, Uchtman and R. A. Gloss, J. Phys. Chem. **76**, 1298 (1972).
[35] V. A. Uchtman, J. Phys. Chem, **76**, 1304 (1972).
[36] E. L. Barnett and L. C. Strickland, Acta Crystallogr. B **35**, 1212 (1979).
[37] J. P. Räsänen, E. Pohjala, H. Nikander, and T. A. Pakkanen, J. Phys. Chem. **100**, 8230 (1996).
[38] J. P. Räsänen, E. Pohjala, H. Nikander, and T. A. Pakkanen, J. Phys. Chem. A **101**, 5196 (1997).
[39] A. E. Reed, R. B. Weinstock, and F. Weinhold, J. Chem. Phys. **83**, 735 (1985).

DOI:10.1088/1674-0068/24/03/295-304